Original Article
Dosimetry of [^{177}Lu]-DO3A-VS-Cys^{40}-Exendin-4 – impact on the feasibility of insulinoma internal radiotherapy

Irina Velikyan[1,2,3], Thomas N Bulenga[1], Ramkumar Selvaraju[1], Mark Lubberink[2,3], Daniel Espes[4], Ulrika Rosenström[1], Olof Eriksson[1]

[1]Department of Medicinal Chemistry, Preclinical PET Platform, Uppsala University, SE-75183 Uppsala, Sweden; [2]PET-Centre, Centre for Medical Imaging, Uppsala University Hospital, Uppsala, Sweden; [3]Department of Radiology, Oncology, and Radiation Science, Uppsala University, SE-75285 Uppsala, Sweden; [4]Department of Medical Cell Biology, Uppsala University, SE-75285 Uppsala, Sweden

Abstract: [^{68}Ga]-DO3A-VS-Cys^{40}-Exendin-4 has been shown to be a promising imaging candidate for targeting glucagon like peptide-1 receptor (GLP-1R). In the light of radiotheranostics and personalized medicine the ^{177}Lu-labelled analogue is of paramount interest. In this study we have investigated the organ distribution of [^{177}Lu]-DO3A-VS-Cys^{40}-Exendin-4 in rat and calculated human dosimetry parameters in order to estimate the maximal acceptable administered radioactivity, and thus potential applicability of [^{177}Lu]-DO3A-VS-Cys^{40}-Exendin-4 for internal radiotherapy of insulinomas. Nine male and nine female Lewis rats were injected with [^{177}Lu]-DO3A-VS-Cys^{40}-Exendin-4 for ex vivo organ distribution study at nine time points. The estimation of human organ/total body absorbed and total effective doses was performed using Organ Level Internal Dose Assessment Code software (OLINDA/EXM 1.1). Six more rats (male: n = 3; female: n = 3) were scanned by single photon emission tomography and computed tomography (SPECT-CT). The renal function and potential cell dysfunction were monitored by creatinine ISTAT and glucose levels. The fine uptake structure of kidney and pancreas was investigated by ex vivo autoradiography. Blood clearance and washout from most of the organs was fast. The kidney was the dose-limiting organ with absorbed dose of 5.88 and 6.04 mGy/MBq, respectively for female and male. Pancreatic beta cells demonstrated radioactivity accumulation. Renal function and beta cell function remained unaffected by radiation. The absorbed dose of [^{177}Lu]-DO3A-VS-Cys^{40}-Exendin-4 to kidneys may limit the clinical application of the agent. However, hypothetically, kidney protection and peptidase inhibition may allow reduction of kidney absorbed dose and amplification of tumour absorbed doses.

Keywords: Lu-177, Exendin-4, dosimetry, insulinoma, imaging, radiotherapy

Introduction

The modern health care is developing towards personalized therapies in order to improve efficacy, efficiency, safety, and quality of patient treatment. Early diagnosis and therapy on molecular level are factors that reduce the mortality and cancer management costs [1]. Positron Emission Tomography (PET) and gamma scintigraphy (Single Photon Emission Computed Tomography (SPECT) and planar gamma imaging) in combination with computed tomography (CT) provide means for cancer staging, and lesion delineation as well as treatment response prediction and monitoring. Together with the subsequent external and internal radiotherapy they merge into theranos-tics of personalized medicine [2]. In nuclear medicine, with the use of radioactive agents targeted at specific biological processes, theranostics can be referred to as radiotheranostics wherein the same ligand is labelled either with imaging (e.g. ^{68}Ga (t$_{1/2}$ = 68 min; β$^+$ [89%])) or radiotherapeutic (e.g. ^{177}Lu (t$_{1/2}$ = 6.67 d; β$^-$ [100%])) nuclide [2]. The diagnosis is conducted for the prediction of the efficacy of specific therapeutic interventions on an individual basis as well as for treatment response monitoring. One more important aspect is pre-therapeutic individual dosimetry for the assessment of potential radiotoxicity to the essential radiosensitive organs, such as bone marrow, organs with a physiological uptake of the radiopharmaceutical and healthy tissue surrounding lesions and

excretory organs. Dosimetry evaluates the distribution and kinetics of an administered radiopharmaceutical [3].

In the case of peptide based agents, the kidney is often a limiting organ and the maximal tolerated absorbed dose must be determined for each individual patient. Thereby the optimal radiotherapeutic dose can be determined and undertreatment as well as nephrotoxicity can be avoided. ^{177}Lu-labelled somatostatin analogues have been used for peptide receptor radionuclide therapy (PRRT) of tumours overexpressing somatostatin receptors (SSTRs) such as neuroendocrine tumours resulting in symptomatic improvement without any severe side effects [4, 5]. The maximum beta particle (E(β^{-}) = 0.497 MeV; 78.7%) range in tissue is 2 mm for ^{177}Lu and the common perception has been that the short range was relevant for the smaller tumours. However, it has been demonstrated that even ^{177}Lu can be efficient for the treatment of larger tumours [6]. In particular, the effectiveness of ^{177}Lu in treatment of neuroendocrine tumours and its favourable dosimetry in kidneys compared to ^{90}Y is well documented [4, 7, 8]. Renal protection using lysine and arginine amino acid solutions is often required. The bone marrow is also an organ at risk. ^{177}Lu emits also gamma radiation that can be used for the simultaneous with PRRT SPECT imaging and dosimetry. However, the accurate assessment of the therapy response might require more sensitive and quantitative technique such as ^{68}Ga/PET-CT.

Insulinomas are clinically characterized by severe symptoms of hyperinsulinism due to unregulated insulin secretion and consequently hypoglycaemia. It is a rare but potentially fatal disease. After the biochemical diagnosis, lesion localization and staging are of paramount importance for adequate patient management. Insulinomas are usually benign and curative surgery is the gold standard treatment if the lesions can be localized. However, with surgery there is always risk for complications and it might not be an option for metastasized insulinomas [9, 10]. Due to the small size of the tumours (82% < 2 cm, 47% < 1 cm), they are often difficult to detect. The diagnosis is only conclusive in < 50% of the cases using widely available conventional radiological procedures (endosonography, magnetic resonance (MR)-, and CT-imaging). Selective angiography can detect lesions in about 60% of the subjects and, in combination with venous sampling for insulin after intra-arterial calcium stimulation administration the accuracy increases to about 60-80%. However, it is an invasive procedure and is accompanied by risks for complications (12). Imaging using metabolic agents such as [^{18}F]FDG/PET-CT, [^{11}C]HTP/PET-CT [11] or [^{18}F]DOPA/PET-CT is not sufficiently sensitive. Even though insulinomas are neuroendocrine tumours, the density of the somatostatin receptors in benign insulinomas is too low for the adequate imaging with respective radioligands, e.g [^{111}In]-pentetreotide (Octreoscan®) that failed to detect the small multiple lesions [11]. In contrast to benign insulinomas, where the exact localization of the tumour is the main goal, the clinical challenge in malignant insulinomas is the accuracy of staging. PRRT might be the treatment of choice, and is a very promising alternative to chemotherapy. One of the advantages is that the radiotherapeutic agents are used in very low mass amounts consequently reducing the side effects.

Insulinomas express glucagon-like peptide 1 receptor (GLP-1R) with high incidence and density and imaging agents based on agonist ligands such as Exendin-3 and Exendin-4 have been developed. In particular, [^{68}Ga]Ga-DO3A-VS-Cys^{40}-Exendin-4 showed high affinity and specificity for GLP-1R expressed on insulinoma cells *in vitro* and *in vivo* distinguishing between pancreatic endocrine tumour (INS-1) and pancreatic exocrine tumour (PANC1) [12]. Targeting GLP-1R with [^{68}Ga]Ga-DO3A-VS-Cys^{40}-Exendin-4 was not only successfully tested preclinically, but also demonstrated promising results in a clinical case examination of a patient affected by metastasized insulinoma [11]. The lesions could not be unambiguously localised by CT, ultrasound, [^{18}F]FDG/PET-CT, [^{11}C]HTP/PET-CT or [^{111}In]-pentetreotide/SPECT-CT, while [^{68}Ga]Ga-DO3A-VS-Cys^{40}-Exendin-4 clearly visualized multiple small lesions in the liver and para-aortal lymph node. Moreover, tumour burden in an insulinoma xenograft model in immunodeficient mice (INS-1), was decreased by administration of a high radioactivity dose of [^{111}In]In-DTPA-Exendin-4 [13].

Given the promising results regarding accurate localization of primary tumour and distant metastases in an insulinoma patient, it is of paramount interest to explore the possibility of

internal radiotherapy using [177Lu]-DO3A-VS-Cys[40]-Exendin-4. However, the development and evaluation of a new radiopharmaceutical is a major undertaking which requires both financial and resource expenditures. Also ethical aspects of animal usage need to be taken into account and it is therefore rational to first investigate the most critical factors influencing the decision of initiating such a study. Thus, the major aim of this study was to conduct dosimetric estimation of [177Lu]-DO3A-VS-Cys[40]-Exendin-4 and assess if the absorbed dose to critical organs may preclude the possibility of internal radiotherapy as well as to estimate the maximum number of radiotherapeutic cycles that could be performed safely without causing radiotoxicity to normal organs. Another aim was to explore the similarity of the distribution pattern of [68Ga]-DO3A-VS-Cys[40]-Exendin-4 and [177Lu]-DO3A-VS-Cys[40]-Exendin-4 and thus the potential of using [68Ga]-DO3A-VS-Cys[40]-Exendin-4 for the pre-therapeutic dosimetry.

Material and methods

Synthesis of DO3A-VS-Cys[40]-Exendin-4

Amino acids (Novabiochem, Switzerland, Alexis Corporation, Switzerland, Iris Biotech GmbH, Germany or Senn chemicals, Switzerland), HBTU (Novabiochem, Switzerland), Cys(Trt) substituted 2-chlorotrityl resin (Senn chemicals, Switzerland), tris-(tert-butyl) ester of DO3A (Sigma-Aldrich, Sweden), piperidine (Sigma-Aldrich, Sweden), NMM (Merck, Germany), DMF (Fisher Scientific, UK).

The side chain protected peptide H_2N-HGEG-TFTSDLSKQMEEEAVRLFIE-WLKNGGPSSGAP-PPSC-OH was synthesized on resin by standard solid-phase peptide synthesis (SPPS). A symphony instrument (Protein Technologies, Inc., Tucson, AZ, USA) was used to synthesis the peptide in 3 batches a´ 50 µmol using Fmoc/tert-butyl (t-Bu) protection. The starting polymer was Cys(Trt) substituted 2-chlorotrityl resin (loading 0.80) and for the Fmoc protected amino acids the side chain protection was as follows: Thr(Ot-Bu), Ser(Ot-Bu), Lys(Boc), Gln(Trt), Trp(Boc), Asn(Trt), Asp(Ot-Bu), Arg(Pbf), His(Trt), Cys(Trt), Glu(Ot-Bu). The Fmoc group was removed by treatment with 20% piperidine in DMF (2 × 2.5 mL) and the amino acids was coupled 30 min using HBTU (500 µmol) in DMF (2.5 mL) in presence of N-methyl morpholine

(NMM, 750 µmol). Double couplings (2 × 30 min) were used for Ile, Val and Arg. After each coupling cycle an N-terminal acetylation was accomplished (20% acetic anhydride in DMF, 5 min), this capping of the unreacted amino groups was performed immediately after deprotection, i.e. without washing. After completion of the coupling steps the Fmoc group was removed and the partially protected peptide on resin was washed with several portions of DMF and CH_2Cl_2, dried in a stream of nitrogen and in vacuum. The peptide was cleaved from the resin and deprotected with TFA/thioanisole/triethylsilane/H_2O (87:4:5:4, 2.5 mL). The reaction mixtures was rotated fore 3 h, filtered and washed with TFA. The solutions were reduced under a stream of nitrogen and precipitated with ether. After centrifugation the ether was removed and the residue was washed with ether and dried under vacuum. The crude material was purified by RP-HPLC (C18, flow rate 10 mL/min, gradient 10-60% CH_3CN in H_2O, 25 min) and selected fractions were analysed by LC-MS and/or RP-HPLC. Those containing pure product were pooled and lyophilized and the pure peptide was obtain in 8% yield (based on initial loading of the resin).

Vinylsulfonyl-DO3A (DO3A-VS) was synthesised in 50 µM scale [14] and conjugateted to Cys[40]-Exendin-4 in a similar way as previously reported [15]. DO3A-VS (2.2 mg, 4.7 µmol) was dissolved in 0.6 mL water and 10 µL 1 M NaOH. Exendin-4-Cys[40] (18 mg, 4.2 µmol) dissolved in 1.4 mL water was added and pH was adjusted to 8 by adding 30 µL 1M NaOH. All the starting material was consumed after 1.5 h according to LC-MS and 0.01% TFA in water (2 mL) was added to the reaction mixture. RP-HPLC was used to purify the crude product (C8, flow rate 5 mL/min, gradient 20-50% in 75 min) and selected fractions were analysed by LC-MS and/or RP-HPLC. Those containing pure product were pooled and lyophilized and the pure compound was obtain in 21% m/z = 2378.15 for $[M+2H]^{2+}$, 1586.43 for $[M+3H]^{3+}$ and 1190.46 for $[M+4H]^{4+}$ with reconstituted molecular weight of 4755.22.

Preparative reversed high-preformance liquid chromatography (RP-HPLC) was performed on a Zorbax SB-C8 column (21.2 × 150 mm) or a Nucleodur C18 Htec 5 µm column (21 × 125 mm) using a CH_3CN/H_2O gradient with 0.1% trifluoroacetic acid (TFA) at a flow rate of 5 mL/

min or 10 mL/min and with UV detection at 220 nm. Analytical RP-HPLC was performed on a Zorbax SB-C8 column (4.4 × 50 mm) or a Nucleodur C18 Htec column (4.6 × 50 mm) using a the same buffer system with a flow rate of 2 mL/min and with UV detection at 220 nm. Analytical electrospray ionization liquid chromatography mass spectrometry (ESI-LC-MS) analysis was performed on a Dionex Ultimate 3000 with a Bruker amaZon iontrap mass spectrometer using a PhenomenexKinetex core-shell C18 (4.6 × 50 mm) 2.6 µm column and a 1.5 mL/min, acetonitrile/water (0.05% formic acid) gradient with positive mode scanning and detecting [M+2H]$^{2+}$, [M+3H]$^{3+}$ and [M+4H]$^{4+}$ species.

Radiochemistry

Hydrochloric acid solution (100 µl, 0.1 M; IDB Holland BV) of ^{177}LuCl$_3$ (630 MBq) was buffered with sodium acetate buffer (pH 4.6). Then aqueous solution (500 µl, 20 µM) of DO3A-VS-Cys^{40}-Exendin-4 and 200 µl ethanol (99.5%) were added and the reaction mixture was incubated at 75°C for 15 min. The product was purified on a solid phase extraction cartridge (HLB Oasis Light) and eluted with ethanol (50%, 1 mL). The resulting [^{177}Lu]-DO3A-VS-Cys^{40}-Exendin-4 was stored at -20°C until use. The quality control was conducted using reverse phase separation by high-performance liquid chromatography (HPLC) on Elite LaChrom system (Hitachi, VWR) consisting of an L-2130 pump, UV detector (L-2400), and a radiation flow detector (Bioscan) coupled in series. Separation of the analytes were accomplished using endcapped analytical column with stationary phase of covalently bonded pentylsilane (Discovery BIO Wide Pore C5; 50 × 4.6 mm). The conditions were as followed: A = 10 mM TFA; B = 70% acetonitrile (MeCN), 30% H$_2$O, 10 mM TFA with UV-detection at 220 nm; linear gradient elution: 0-2 min at 35% B, 2-9 min at 35 to 100% B, 9-12 min at 100% B ; flow rate was 2.0 mL/min. Data acquisition and handling were performed using the EZChrom Elite Software Package. The analyte sample was prepared in 5 mM EDTA solution. The radioactivity recovery from the analytical column was controlled by performing analysis with and without column and collecting the fractions for the subsequent measurement of the radioactivity in a well-type NaI(Tl) scintillation counter corrected for dead-time and for radioactive decay.

Organ distribution in rats

Ex vivo organ distribution of [^{177}Lu]-DO3A-VS-Cys^{40}-Exendin-4 was studied in healthy female (n = 9; 203.9 ± 7.5 g) and male (n = 9; 191.7 ± 18.4 g) Lewis rats. The permission was granted by the local Research Animal Ethics Committee. The animals were kept at a constant temperature (25°C) and humidity (50%) in a 12 h light-dark cycle. Food and water were given *ad libitum*. [^{177}Lu]-DO3A-VS-Cys^{40}-Exendin-4 was administered (3.3-13.8 kBq; 0.13 ± 0.04 µg/kg) into the tail vein of unsedated animals as a bolus in 0.5-0.6 mL of phosphate buffered saline (pH 7.4) as the vehicle. One rat of each gender was sacrificed after 0.17, 0.5, 1, 3, 8, 24, 72, 168, and 336 h respectively. Organs were immediately extracted, their radioactivity measured in a well-type NaI(Tl) scintillation counter, applying correction for dead-time and for radioactivity decay, and the mass of the extracted tissues was determined. The remaining carcas was also measured in order to monitor the radioactivity elimination and recovery. The investigated organs were: blood, heart, lung, liver, pancreas, spleen, adrenal, kidney, small intestine (without/with its content), large intestine (without its content), feces, urinary bladder, testis/ovary, muscle, bone, bone marrow, thyroid and brain. The readings were decay-corrected to the time of injection, and results were expressed as standardized uptake values (SUV) according to **Equation 1** where the radioactivity of an organ and injected radioactivity was expressed in [MBq] and the weight of a rat and organ was expressed in [g].

$$SUV = \frac{Radioactivity_{organ} * weight_{rat}}{Radioactivity_{injected} * weight_{organ}} \quad (1)$$

SPECT-CT imaging

Whole body scan of Lewis rats (n = 3, female, 218.67 ± 10.02 g), injected with ^{177}[Lu]-DO3A-VS-Cys^{40}-Exendin-4 (11.13 ± 3.64 MBq, 0.9 ± 0.3 µg/kg), was performed in Triumph™ Trimodality System (TriFoil Imaging, Inc., Northridge, CA, USA) at time points 1, 24 and 168 h post injection (p.i.). A higher radioactivity dose in MBq, and subsequently in µg peptide/kg compared to the organ distribution study, was administered in order to enable detection of the counts by the less sensitive SPECT instrument. Subjects were euthanized by CO$_2$ just before placing them in the scanner. The SPECT

scan was performed in helical mode covering from head till tail of the subjects using a 65A10 five pinhole collimator, at a radius-of-rotation (ROR) of 50 mm for 140 minutes with 64 projections at 131 seconds per projection. Following the SPECT scan, a whole body CT was obtained by merging 3 consecutive scans at magnification 1.3, covering a total of 180 mm using TriFoils stitching module in AMIRA 5.6 (FEI Visualization Sciences Group, MA, USA). SPECT raw data was reconstructed by an Ordered Subset Expectation Maximization (OSEM) iterative reconstruction algorithm in the FLEX SPECT software. CT raw files were reconstructed by Filter Back Projection (FBP). SPECT and CT data were fused an analyzed in PMOD 3.58 (PMOD Technologies Ltd., ZRH, Switzerland).

Ex vivo autoradiography

Lewis rats (n = 3, male, 295.7 ± 2.5 g) were administered 9.77 ± 4.41 MBq corresponding to 0.79 ± 0.35 µg peptide/kg. The animals were euthanized by CO_2 1, 24 and 168 h p.i. Kidneys and pancreas were removed post mortem and sectioned by a microtome (Microm 560 cryostat, cellab Nordia Ab, Sweden) into 20 µm sections and placed upon object glasses. The object glasses from each animal were exposed against SR (Super Resolution) storage phosphor screens (PerkinElmer, Downers grove, IL, USA), for 1-2 h together with a known reference of 15 kBq to allow for direct comparison between different time points. The plates were scanned using a Cyclone plus phosphor imager (PerkinElmer, Model no C431200, Downers grove, IL, USA).

The pancreatic sections were immediately re-frozen and later thawed and stained for insulin by the immunofluorescencemethod (IF). The sections were fixed in ice-cold acetone for 10 minutes and then washed in PBS for 3 minutes, followed by incubation with DAKO Serum free protein block (Agilent Technologies, Glostrup, Denmark) for 30 minutes. The sections were then incubated over night at 4°C in the insulin primary antibody (Insulin A, Santa Cruz, SC-7839, goat-polyclonal (1:1000) followed by wash in PBS (3 × 3 min). Slides were then incubated with secondary antibody Alexa fluor 488 (Invitrogen, Carlsbad, CA, USA; donkey anti-goat; dilution 1:100) for 60 minutes in a humidified dark chamber, again followed by washin PBS (3 × 3 min). ProLong® Gold Antifade reagent with DAPI (Life Technologies, Rockville,

MD, USA) was used for mounting slides and nuclei staining. Tile scan images were acquired with a Zeiss LSM780 confocal microscope at 10x magnification.

The autoradiograms and the IF stains were analysed and co-registered using ImageJ 1.48v (National Institutes of Health, Bethesda, MD, USA).

Blood glucose and renal function

For the animals used for SPECT-CT imaging and *ex vivo* autoradiography, we assessed blood glucose and creatinine. These measurements were taken to assess potential dysfunction in tissues with high uptake of the tracer i.e. pancreatic beta cells (express GLP-1R) and kidney cortex (trapping of radiometals during excretion) due to acute radiation exposure from ^{177}Lu. Blood glucose value was collected using a Bayer COUNTER monitoring unit (Bayer AG, Apotek, Uppsala, Sweden) in blood from the tail vein from conscious animals. Creatinine in whole blood was measured using the Creatinine/CREA kit (iSTAT, Abbott Point-of-Care, USA).

Dosimetric calculations

Human organ and total body absorbed and effective dose estimates were calculated according to the Medical Internal radionuclide dose (MIRD) procedure using the measured residence times and the dose rate S-values [16, 17]. The SUV values in rat were first multiplied with the appropriate radioactivity decay factor dependent on the time point of the data post-injection, then multiplied by standard organ masses and divided by the standard total-body weight for the standard adult man phantom obtained from the OLINDA/EXM 1.1 software (Organ Level Internal Dose Assessment Code, Vanderbilt University, USA, 2007) [18]. The values obtained correspond to the fraction of injected radioactivity (%IA) per organ in man as a function of time (**Equation 2**, where SUV_A is SUVs of rat organs; g_{organ} and $kg_{TBweight}$ are respectively standard organ weight and standard total body weight of a human).

$$(\%IA_{Organ})_{human} = SUV_A * \left(\frac{g_{organ}}{kg_{TBweight}}\right)_{human} \quad (2)$$

The cumulative radioactivity for the organs was determined by integrating the area under the
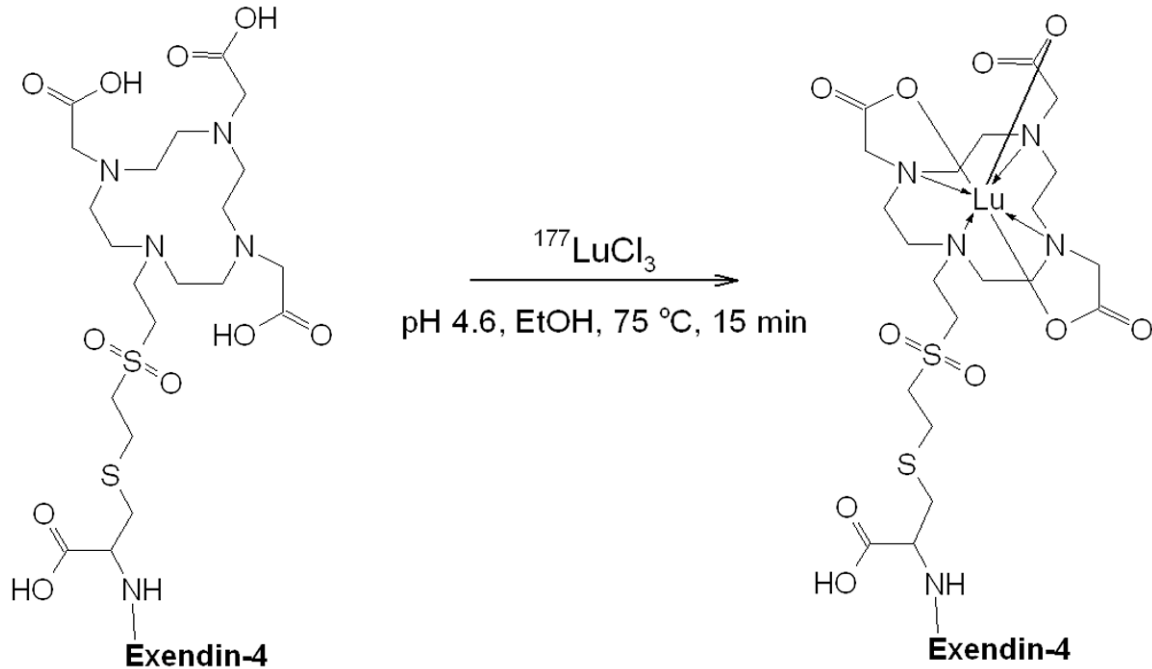
Figure 1. Schematic representation of ^{177}Lu-labelling of DO3A-VS-Cys^{40}-Exendin-4; Exendin-4: HGEGTFTSDLSKQ-MEEEAVRLFIEWLKNGGPSSGAPPPS.

Table 1. Animal weights and injected radioactivity doses

Gender	N	Animal weight, [g]	Injected dose, [MBq]
Male (organ distribution)	9	192 ± 18	1.7 ± 0.6
Female (organ distribution)	9	204 ± 8	1.5 ± 0.6
Female (SPECT-CT imaging)	3	219 ± 10	11.1 ± 3.6
Male (autoradiography)	3	296 ± 3	9.8 ± 4.4

time-radioactivity curves for each organ using trapezoidal approximation of the collected kinetic data, followed by extrapolation of remaining points from the last time point to infinity by a single exponential fit. The residence time for each organ is equal to the number of disintegrations (MBq*h/MBq). Bone marrow residence time was assessed according to the bone marrow blood model [19]. The residence time for the remaining carcass was calculated in the same way as for the other organs and this value was used as input in the OLINDA software as "Remainder". "Remainder" of the body residence time was calculated from SUV due to radioactivity measured in the rest of the body after the removal of the source organs and tail. The difference between the theoretical residence time and the calculated residence time of the source organs plus remainder of the body was assumed to have been in the tail or excreted. The kidney absorbed dose was calcu-lated based on multi-region kidney model phantom [20]. The total target organ absorbed dose (*D*) is contributed by all source organs and is expressed by **Equation 3**, where Ã is the time-integrated radioactivity in the source tissue (r_s) and *S* is the radionuclide-specific dose rate values [16]:

$$D\,(r_T, t) = \sum r_S\,\widetilde{A}\,(r_S, t) * S(r_T \leftarrow r_S, t) \qquad (3)$$

Statistics

Average values (mean) and their corresponding standard deviation (SD) were calculated with Excel (Microsoft) or GraphPad Prism version 5.0 (GraphPad Software, San Diego, California, USA). Non-linear regression analyses were made with GraphPad Prism and the goodness of fit to the variables was presented as R^2 values.

Results

Radiochemistry

The long half-life and high concentration of ^{177}Lu provides the possibility for the high spe-
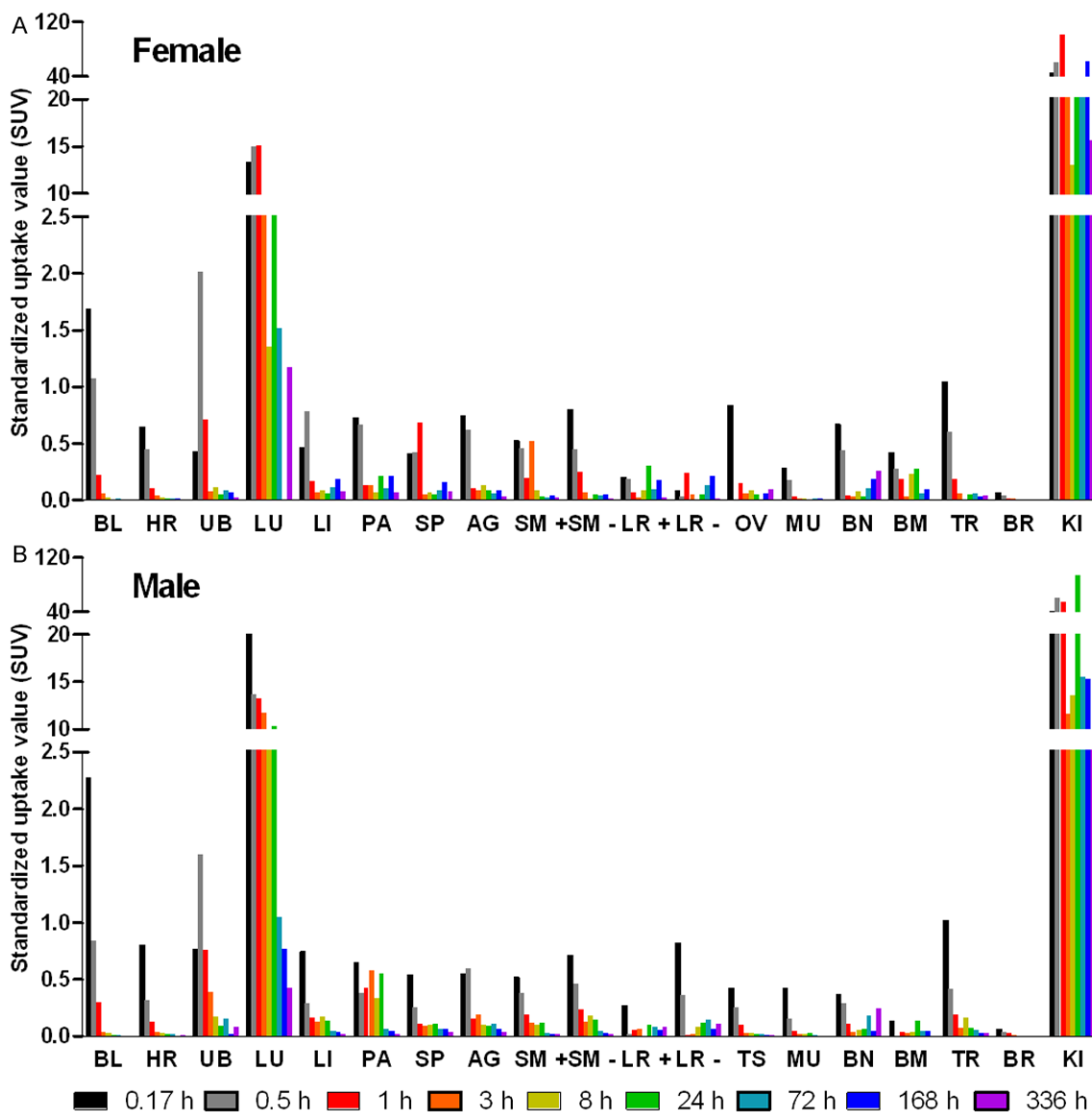
Figure 2. Graph, summarizing the distribution in 19 rat organs of [^{177}Lu]-DO3A-VS-Cys^{40}-Exendin-4 administered intravenously. Nine female (A) and nine male (B) animals received the tracer. BL: blood; HR: heart; UB: bladder; LU: lungs; LI: liver; PA: pancreas; SP: spleen; AG: adrenal gland; SM+: small intestine with its content; SM–: small intestine without its content; LR+: large intestine with its content; LR–: large intestine without its content; OV: ovaries; TE: testes; MU: muscle; BN: bone; BM: red bone marrow; TR: thyroid; BR: brain; KI: kidneys.

cific radioactivity (SRA = 1.3 ± 0.05 GBq/nmol) and thus on one hand injection of low peptide amount taking into consideration the strong potency of it, and on the other hand sufficient radioactivity for the statistics of counts. However, lower amount of radioactivity was used in order to adjust the amount of the injected peptide to the one usually achieved when using ^{68}Ga. The radioactivity incorporation was over 95% with radiochemical yield of 72 ± 5% due to the losses on the solid phase extraction cartridge during product purification. Ten per-

cent (volume) of ethanol was added to the reaction mixture in order to suppress the radiolysis (**Figure 1**). The HPLC analysis required addition of EDTA to the analyte solution in order to complex ionic ^{177}Lu(III) and maintain the analytical column recovery over 95%. Otherwise, ^{177}Lu(III) was retained on the column resulting in false high radiochemical purity value.

Organ distribution and kinetics

A total of 18 rats (9 female and 9 male, **Table 1**) were injected with [^{177}Lu]-DO3A-VS-Cys^{40}-Exen-
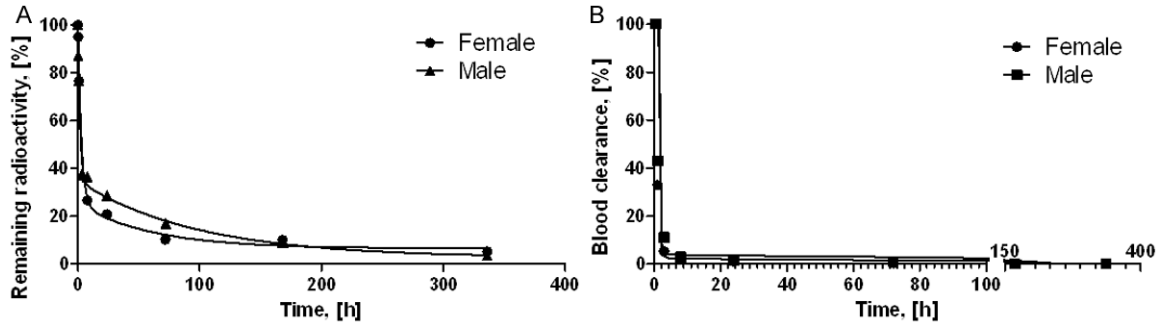
Figure 3. Graphs showing the elimination kinetics (A, R^2 = 0.9952 (female) and 0.9902 (male)) and blood clearance (B, R^2 = 0.9986 (female) and 0.9943 (male)) of [^{177}Lu]-DO3A-VS-Cys^{40}-Exendin-4 administered intravenously.
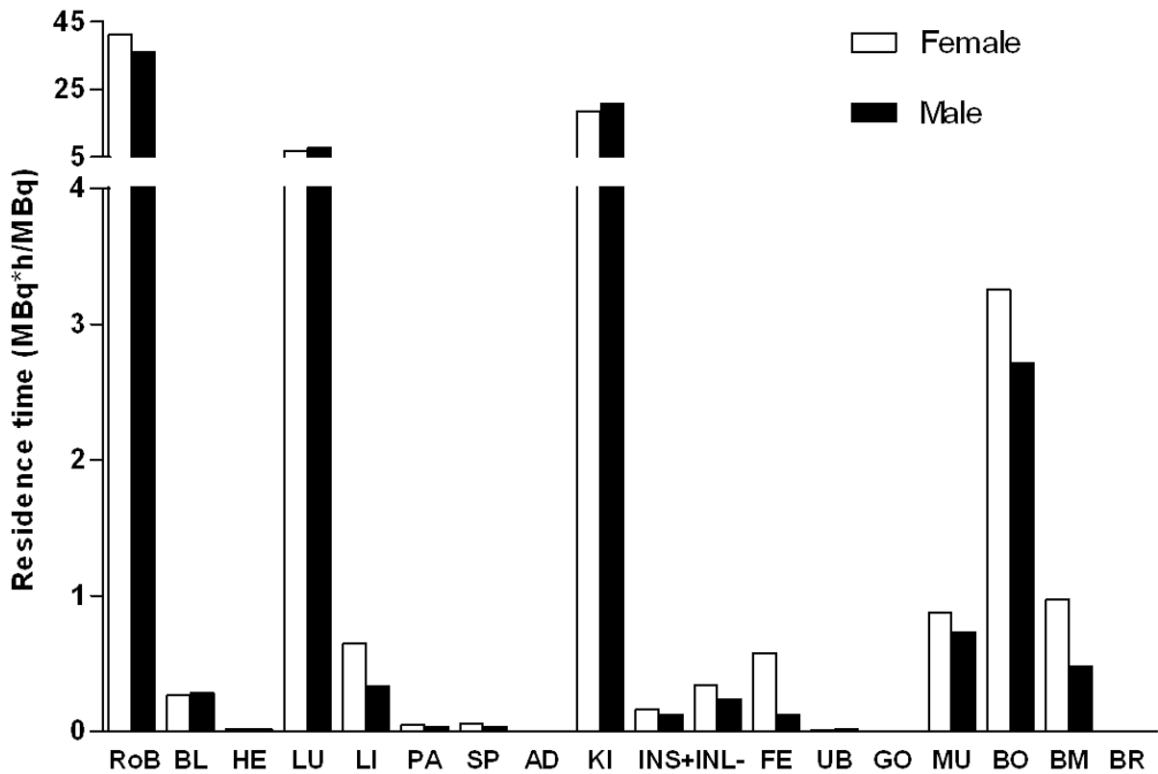

Figure 4. Graph showing the residence times of [^{177}Lu]-DO3A-VS-Cys^{40}-Exendin-4 in different organs. The values were extrapolated to human female and male from rat *ex vivo* organ distribution data, and used for dosimetric calculations using OLINDA/EXM 1.1 software. It should be noted that the values for "Rest of body" were determined for all animal-associated radioactivity that was not in the excised and measured organs. RoB: rest of body; BL: blood; HE: heart; LU: lungs; LI: liver; PA: pancreas; SP: spleen; AD: adrenals; KI: kidneys; INS+: small intestine with its content; INL: large intestine without content; UB: bladder; GO: gonades; MU: muscle; BO: bone; BM: red bone marrow; BR: brain.

din-4. The specific radioactivity of [^{177}Lu]-DO3A-VS-Cys^{40}-Exendin-4 at the end of the synthesis was 27 ± 2 MBq/nmol. The injected peptide amount was 0.13 ± 0.04 µg.

The organ distribution of [^{177}Lu]-DO3A-VS-Cys^{40}-Exendin-4 was performed in 19 organs and

presented as decay-corrected SUV values (**Figure 2**). [^{177}Lu]-DO3A-VS-Cys^{40}-Exendin-4 showed a relatively fast clearance from blood to tissue (SUV in blood was < 0.3 1 h p.i.) and displayed a pronounced wash-out pattern from most of the organs (SUV < 1). The high kidney uptake (SUV > 10) indicated renal excretion

both in male and female rats. The elimination was determined together with the remaining radioactivity (not excreted) for each animal and time point (0.17, 0.5, 1, 3, 8, 24, 72, 168, and 336 h). The radioactivity was rapidly eliminated in both genders. The elimination kinetics was best described by a two-phase exponential with slow and fast phases of half-life 42.12 and 1.95 h for females and 67.99 and 1.12 h for males (**Figure 3A**; R^2 = 0.9952 and 0.9902). Only 5.3% (female) and 3.5% (male) of the injected radioactivity remained in the animals 336 h after administration. The elimination kinetics was similar for the female and male with relative standard deviation for the half-lives with only 16 and 19%, respectively for slow and fast phases. The blood clearance was calculated with respect to 0.5 h time point and was rapid for both females and males with less than 1.0% of remaining radioactivity 72 h p.i.. The clearance kinetics was best described by a single exponential phase (**Figure 3B**; R^2 = 0.9986 (female); 0.9943 (male)), accounting for 99% of the radioactivity, followed by a linear phase. The half-life for the clearance was 0.300 h and 0.395 h, respectively for females and males. The radioactivity was considerably diminished after 72 h in most of other organs except for the kidneys and lungs where wash-out was slow in both genders (**Figure 2**).

The reliability of the results was accessed by the goodness of the mathematical function fit using larger number of data points (9 time points) rather than using fewer data points with several replicates. The advantage of larger number of data points is more accurate description of the process and much lower number of sacrificed animals. Such approach can be justified by high R^2 values and low percentage or absence of outlying points. The main aim of the measurements was the determination of the cumulated radioactivity which is determined by the integration of the area under the curve. The mathematical functions fit the data points with high R^2 values (0.9947 ± 0032, N = 4, **Figure 3**) indicating accuracy of the measurements. Despite of gender the pattern of distribution kinetics was similar with rapid radioactivity elimination and blood clearance. Due to the accuracy of the results, ethical considerations discouraged us from increasing the amount of animals that would be sacrificed unnecessarily in the experiment.

Dosimetry

The extrapolation of the rat biodistribution data to human species for the calculation of the absorbed and total effective doses was conducted with two basic assumptions: 1) similarity of the biodistribution pattern in human and rat; 2) homogeneous distribution of radioactivity throughout the organ [18]. The organ distribution study was conducted for 336 h while theoretical residence time for ^{177}Lu(III), assuming retention in the organism for its whole physical life-span is approximately 230 h. Residence time, which theoretically equals to the area under the organ time radioactivity curves from time zero to infinity, was calculated applying the trapezoidal rule allowing calculation of the residence time using the area from the injection time to the termination time. The basic assumption is that the further decline in radioactivity occurs due to physical decay without further biological clearance. [^{177}Lu]-DO3A-VS-Cys^{40}-Exendin-4 residence time results are summarized in **Figure 4**. The longest residence times were observed for the remaining body, followed by kidneys, lung, and bone with values similar for male and female.

Absorbed doses and total effective doses were calculated using residence time values as input into OLINDA/EXM 1.1, MIRD scheme of an adult male (70 kg) [17], and recommended tissue weighting factors from International Commission on Radiological Protection (ICRP, 2007). The absorbed doses (mGy/MBq) and total effective doses (mSv/MBq) obtained from OLINDA/EXM 1.1 calculations are presented in **Table 2**. The extrapolated absorbed dose for [^{177}Lu]-DO3A-VS-Cys^{40}-Exendin-4 was highest in kidneys for both female and male. The absorbed dose for lungs was highest amongst the remaining organs. The total effective dose was 0.295 and 0.265 mSv/MBq, respectively for female and male. Interestingly, the absorbed doses were slightly higher for females than for males for practically all organs.

SPECT-CT imaging

At all time points, kidneys dominated the whole body images as the tracer excretory organ and the slower extravasation was evident at later time points (**Figure 5**). Lungs could be delineated at the first time point, 1 h p.i., and showed faster clearance with time. Tracer uptake was in accordance with organ biodistribution stud-

Table 2. Estimated absorbed doses (mGy/MBq) of [^{177}Lu]-DO3A-VS-Cys^{40}-Exendin-4 in human females and males extrapolated from rat organ distribution data

ORGAN	FEMALE	MALE
Kidneys	5.880	6.040
Adrenals	0.051	0.041
Liver	0.053	0.026
LLI wall*	0.071	0.049
ULI wall**	0.075	0.052
Red marrow	0.117	0.081
Spleen	0.058	0.036
Osteogenic cells	0.484	0.303
Small intestine	0.093	0.065
Ovaries/Testes	0.031	0.007
Urinary Bladder Wall	0.071	0.050
Breasts	0.068	NA
Uterus	0.071	NA
Stomach wall	0.076	0.053
Thymus	0.071	0.049
Thyroid	0.068	0.047
Gall bladder wall	0.078	0.056
Skin	0.066	0.045
Lungs	0.752	0.676
Heart wall	0.018	0.013
Muscle	0.013	0.009
Pancreas	0.067	0.051
Brain	0.069	0.047
Total body	0.119	0.088
Total effective dose (mSv/MBq)	0.295	0.265

*LLI: lower large intestine; **ULI: upper large intestine.

ies except for lower lung uptake. Here also kidney was suggested the dose limiting organ. Rapid blood clearance, and no uptake in liver and spleen clearly indicated the stability of tracer *in vivo*, absence of free ^{177}Lu for transchelation to serum proteins and nearly no possibility for radiocolloid formation in the subject with time.

Ex vivo autoradiography

The uptake in kidneys was concentrated to the kidney cortex as expected (**Figure 6C**, **6F** and **6I**). The cortex uptake was at its highest already after 1 h and plateaued until 24 h. A decrease was seen at 168 h, consistent with the results seen by SPECT-CT imaging and the biodistribution study. The pancreatic uptake was concentrated in a distinct focal pattern throughout the organ (**Figure 6B**, **6E** and **6H**). Staining of the

sections showed that the uptake was co-registered with insulin (**Figure 6A**, **6D** and **6G**). This is consistent with the notion that GLP-1R is predominantly expressed in the pancreatic beta cells in rat.

Blood glucose and renal function

Blood glucose levels did not show any considerable change after injection of [^{177}Lu]-DO3A-VS-Cys^{40}-Exendin-4, at any time point (**Table 3**). A similar pattern was observed with blood creatinine values showing that the radiation exposure from ^{177}Lu-labelled tracer in kidney did not affect the renal function (**Table 3**) during the first week following the doses administered here.

Discussion

The exploration of the potential of [^{177}Lu]-DO3A-VS-Cys^{40}-Exendin-4 for PRRT in patients affected by insulinomas, which are normally small in size (< 2 cm) [9, 10], was inspired by: 1) accurate localization of primary tumour and distant metastases using [^{68}Ga]-DO3A-VS-Cys^{40}-Exendin-4 in an insulinoma patient [11]; 2) experience with ^{177}Lu-labelled somatostatin analogues used in PRRT of NETs that demonstrated promising results in terms of patient survival duration. The first step was the investigation of the dosimetry since it is well established knowledge that in most of the cases the kidneys and bone marrow are organs at risk in PRRT with peptide based agents. The major aim of the dosimetry and subsequent administered dose planning is to minimize radiotoxicity to healthy tissue/organs on one hand and to avoid undertreatment on the other hand. The usefulness of extrapolation of animal organ biodistribution data to the human organ and whole-body radiation dosimetry has been demonstrated previously, e.g. for radiolabelled somatostatin analogues [21-23]. The translation might be accompanied by the biodistribution variation between different species, e.g. rats, mice [22, 24] and human. Nevertheless, the absorbed doses to kidneys estimated in an animal study [21] and obtained from a clinical study [25] correlated.

Rat biodistribution and human absorbed dose estimates

The optimization of the PRRT protocol requires maximal enhancement of the absorbed dose to the tumour lesions. The respective adminis-
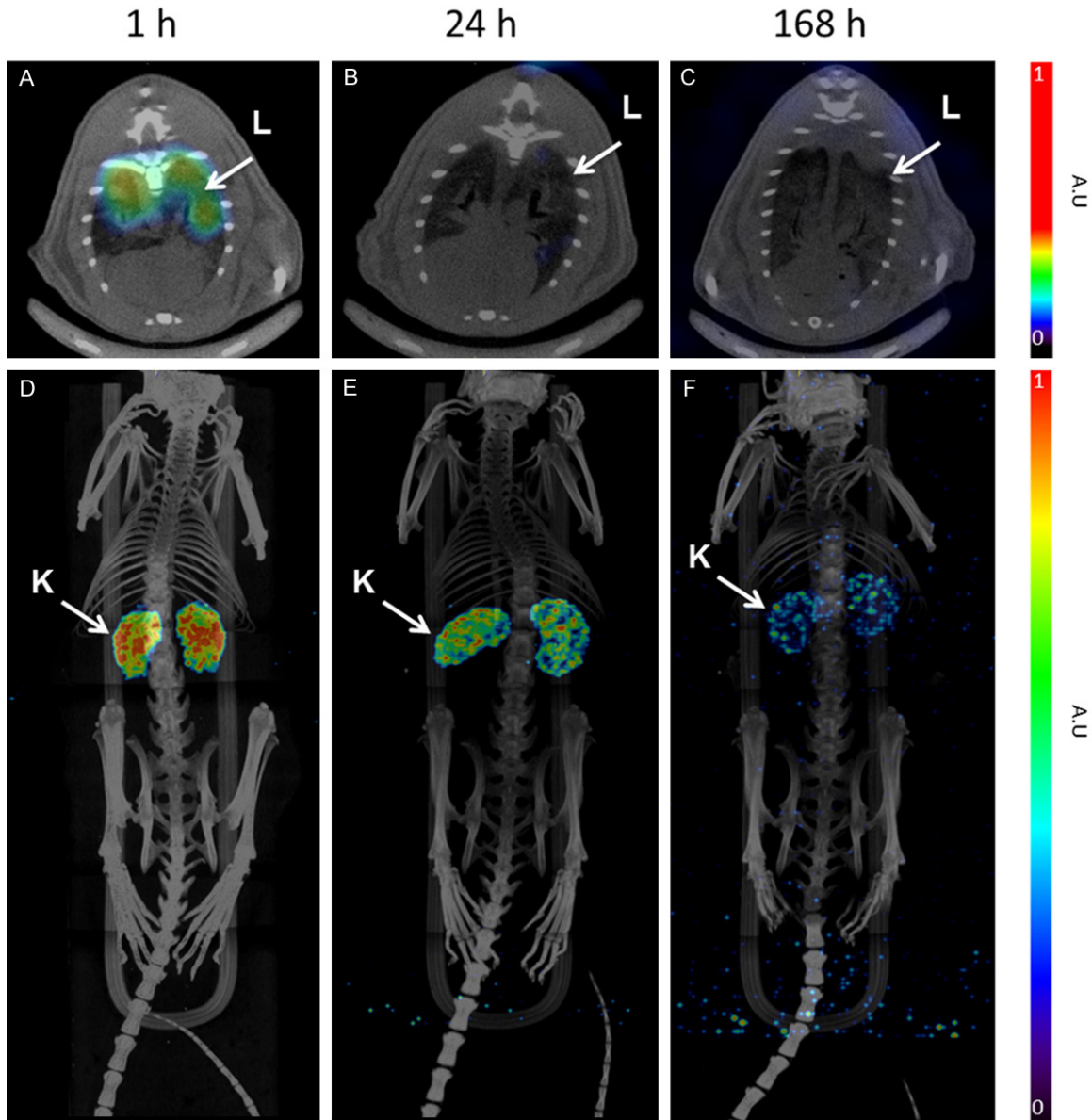
Figure 5. Representative fused SPECT-CT images of [^{177}Lu]-DO3A-VS-Cys^{40}-Exendin-4 in rats at different time points. Lungs could be outlined at 1 h p.i. and showed faster clearance in later time points (A-C). MIP images (D-F) of whole body scan showing dominance of kidneys, as excretory organ of tracer, demonstrated slower clearance in later time points. The images were acquired using identical SPECT protocols allowing for comparison. However, the images are not quantitative and the units are given as arbitrary units (A.U.).

tered radioactivity dose is restricted by the absorbed dose to normal organs which must be kept within the maximum tolerated dose for the organs at risk such as bone marrow and kidneys.

[^{177}Lu]-DO3A-VS-Cys^{40}-Exendin-4 was washed out from most of the organs except for lung and kidney within 72 h presumably through renal excretion (**Figures 2**, **3** and **5**). Blood clearance

was fast and without radioactivity deposition in the tissue. No accumulation in red bone marrow occurred and retention was low (0.011%IA/g (male) and 0.016%IA/g (female) 3 h after injection). The absorbed dose to bone red marrow was not the restricting parameter. It was 0.117 mGy/MBq and 0.081 mGy/MBq, respectively for female and male which yielded 20 GBq able to provide up to several therapy cycles before reaching red marrow limiting dose of 2 Gy.
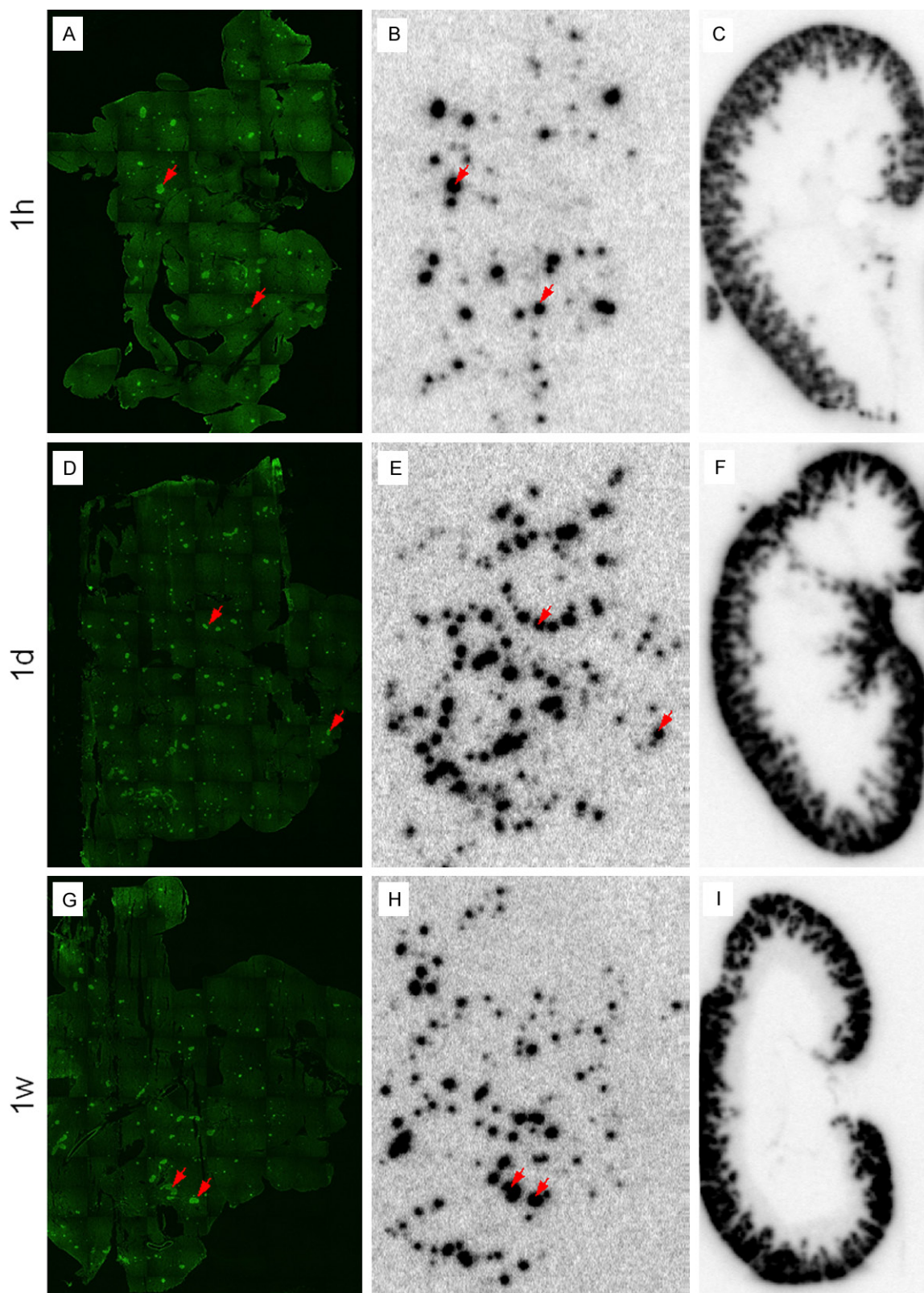
Figure 6. *Ex vivo* autoradiography of kidney and pancreas at 1 h (upper panel), 24 h (middle panel) and 168 h (bottom panel) p.i. Kidney uptake is concentrated to the cortex (C, F, I). The uptake in pancreas is highly focal (B, E, H) and co-registered with insulin as determined by immunofluorescent staining (A, D, G). The pancreatic autoradiograms (B, E and H) are normalized to the same reference and therefore directly comparable. The same normalization was performed for the kidney autoradiograms (C, F and I).

Table 3. Comparison of blood glucose and creatinine values before and after injection of [^{177}Lu]-DO3A-VS-Cys^{40}-Exendin-4 at different time points

Time points [h]	Blood glucose [mmol/L]		Blood creatinine [µmol/L]	
	Before Injection	After Injection	Before Injection	After Injection
1	5.80 ± 0.14	7.65 ± 0.07	39 ± 4.24	33.0 ± 0.00
24	4.65 ± 0.78	5.75 ± 0.35	34.5 ± 3.54	30.5 ± 13.43
168	5.75 ± 0.07	4.70 ± 1.98	33 ± 1.41	36.5 ± 0.71

Similar values for absorbed dose in red marrow have been reported for ^{177}Lu-SST analogues [4, 26, 27]. The remaining rather small fraction of radioactivity was distributed throughout organs with longer retention in lung and kidney. Although washout from these organs was slower, there was only 2.7% IA/g (male) and 7.2% IA/g (female) left at 336 h time point in the kidneys, and 0.2% IA/g (male) and 8.6% IA/g (female) in the lungs.

Significant amount of GLP-1R in rodent lung [28], as well as high displaceable uptake of radiolabeled Exendin-4 [12] has been reported previously. GLP-1R in human lung has also been reported, but not in the same extent as in rodents [29] and there is only minor uptake of radiolabeled Exendin-4 in large animals and humans at all time points [11, 30]. Although GLP-1R expression has been reported in renal cortex, this signal drowns in the radioactive signal originating from excreted radiotracer. The kidney cortex uptake of ^{68}Ga-labelled Exendin-4 was not displaceable [11, 30] and the same is most likely true for the results presented here. The fast clearance from the blood and most of the healthy organs was confirmed by *in vivo* SPECT-CT imaging at 1, 24 and 168 h p.i. (**Figure 5**). The accumulation in the lungs could be observed at 1 h but not at 24 h time point. This is likely due to lower lung uptake in this particular animal.

The pancreatic uptake was relatively low (SUV < 1), despite known high expression of GLP-1R in the beta cells of the islets of Langerhans. This is not unexpected, since the beta cells constitute approximately 1% of the pancreatic volume. Thus, a beta cell specific uptake in the magnitude of SUV = 50 would be diluted by a factor of 100 to a pancreatic SUV of approximately 0.5, which is seen here. A beta cell specific uptake in a similar range was previously seen using ^{68}Ga-labelled Exendin-4 [30]. The pancreatic focal radioactivity uptake unsurpris-

ingly co-registered with insulin distribution as determined by IF staining, confirming GLP-1R expression in the pancreatic beta cells. The estimated pancreatic absorbed dose was low, but this assumes homogenous distribution of the radionuclide in the tissue. The radiation dose to the islets of Langerhans is therefore greatly underestimated and probably many times higher than that estimated for the pancreas as a whole. It is therefore imperative to closely monitor beta cell function in future radiotherapy trials using GLP-1R targeting agents. We observed no acute diabetogenic effects during the first week after administration. However, this does not preclude subclinical effects leading to later beta cell dysfunction. The domination of kidney uptake and slower excretion at later time points reflected the two-phase exponential elimination kinetics determined from organ distribution experiments. More detailed *ex vivo* autoradiography investigation of radioactivity distribution within the kidney frozen section revealed concentrated uptake in the cortex (**Figure 6C**, **6F** and **6I**) indicating that the long retention of the kidney radioactivity was mostly probably due to tubular reabsoption of the peptide [31]. Despite the long retention time of the radioactivity in the kidneys, the renal function in rats was not acutely affected as demonstrated by the monitoring blood creatinine (**Table 3**).

The residence time was 20 MBq*h/MBq in kidneys followed by lungs with 7 MBq*h/MBq for both female and male (**Figure 4**) yielding respectively higher absorbed doses of [^{177}Lu]-DO3A-VS-Cys^{40}-Exendin-4 in these organs as compared to the rest of source organs (**Table 2**). The results indicated that kidney was the dose-limiting organ with an absorbed dose of 5.880 and 6.040 mGy/MBq, respectively for female and male. The maximum total amount of radioactivity of [^{177}Lu]-DO3A-VS-Cys^{40}-Exendin-4 that could be administered to a subject, if solely restricted by the dose absorbed by kidneys, would be 3.9 and 3.8 GBq, respectively for females and males, for one radiotherapy cycle before reaching a kidney tolerable absorbed dose of 23 Gy. This tolerated radioactivity amount is lower compared to commonly

used radioactivity dose of 7.4 GBq in PRRT with ^{177}Lu-SST analogues [25]. However, the radio-therapeutic radioactivity dose is selected individually and even lower amount down to 3.7 GBq for one cycle might be effective [4].

The kidney is often the limiting organ in PRRT with peptide based agents due to predominately renal excretion. In order to minimize kidney toxicity various renal uptake reducing agents have been investigated and are in clinical use [4, 32-35]. Clinical studies have shown that the renal uptake of [^{177}Lu]-DOTA-TOC can be reduced by 20-50% [36, 37]. This approach has been evaluated also for ^{111}In-labelled Exendin-4 in rat models, in which the renal uptake could be reduced by 48% by a combination of polyglutamic acid (PGA) and Gelofusine (GF) [36]. Assuming reduction of the residence time by 48%, we estimated that the absorbed dose of [^{177}Lu]-DO3A-VS-Cys^{40}-Exendin-4 to kidney in human using rat extrapolated residence times could be reduced to approximately 3.1 mGy/MBq. This would potentially allow administration of up to 7.4 GBq of [^{177}Lu]-DO3A-VS-Cys^{40}-Exendin-4 and thereby permitting one cycle of radiotherapy. Once again, it is worth mentioning that the absorbed dose might vary considerably between individuals due to high interpatient variability in healthy organ uptake, e.g. some patients could tolerate over 4 cycles of 7.4 GBq before reaching the limit of 23 Gy, and moreover the latter could be increased up to 29 Gy [25]. The limit of 29 Gy and kidney protection would allow administration of 9.3 GBq in the case of ^{177}Lu]-DO3A-VS-Cys^{40}-Exendin-4. In addition the radiopharmaceutical distribution to the healthy organs is dependent on the tumour burden, which in fact decreases the kidney uptake [38]. Thus even higher administered radioactivity doses might be required in order to prevent undertreatment.

Another plausible reason for the high kidney uptake might be the metabolism of the ligand. Recent studies have demonstrated remarkable improvement of the *in vivo* stability and xeno-grafted tumour uptake of somatostatin, gastrin, and bombesin radiopeptides by co-injection of phosphoramidon (PA) acting as an inhibitor to neutral endopeptidase (NEP) [39]. For example, the fraction of intact somatostatin analogue was increased from 2% to 86% and the tumour uptake increased from 1% to 14%. Such magnification of the radiopharmaceutical

accumulation in the tumour lesions is expected to considerably improve the radiotherapeutic efficacy. The potential role of NEP for the catabolism of glucagon like peptides has been identified *in vitro* [40]. The hydrolysis of Exendin-4 was slowest amongst the analogues, however *in vivo* investigation still indicated rather fast metabolism of Exendin-4 ($t_{1/2}$ = 22 min) [41]. Another study demonstrated that up to 50% of GLP-1 in the circulation might be degraded by NEP, and metabolic stability was improved upon inhibition of NEP and dipeptidyl peptidase IV *in vivo* in pigs [42]. The kidney was presumably identified as an organ mediating the final elimination of the catabolites [41] and thus the improved stability may decrease the kidney uptake and absorbed dose.

Preliminary estimation of tumour absorbed dose, based on a case examination of a patient affected by insulinomas using [^{68}Ga]-DO3A-VS-Cys^{40}-Exendin-4 [11], demonstrated necessity of kidney protection and tumour accumulation enhancement if [^{177}Lu]-DO3A-VS-Cys^{40}-Exendin-4 is to be used. A tumour SUV of 5 was observed at 2 h p.i. and assuming a constant SUV value also at later time points as well as similar tumour accumulation as for [^{177}Lu]-DO3A-VS-Cys^{40}-Exendin-4, this would have resulted in a tumour absorbed dose of 0.7 mGy/MBq. For an injection of 3.7 GBq, this would have given an absorbed dose to the tumour of 2.7 Gy, which might not be sufficient for tumour control. However, potential enhancement of the administered radioactivity up to 9.3 GBq due to the protection of kidneys as mentioned above would increase the tumour absorbed dose to 6.5 Gy. Furthermore, the blood circulation of [^{177}Lu]-DO3A-VS-Cys^{40}-Exendin-4 might be prolonged by the NEP inhibition. This would increase the agent availability for the tumour uptake and consequently tumour absorbed dose. The kidney protection and peptidase inhibition means may allow considerable amplification of the tumour absorbed doses and achievement of radiotherapeutic efficacy. However, it remains to be proven in extensive further investigations.

Potential of ^{68}Ga for pre-therapeutic dosimetry

Development of radiopharmaceuticals for clinical use considers applications for *in vivo* pre-therapeutical dosimetry and administered radioactivity dose planning. ^{177}Lu emits also
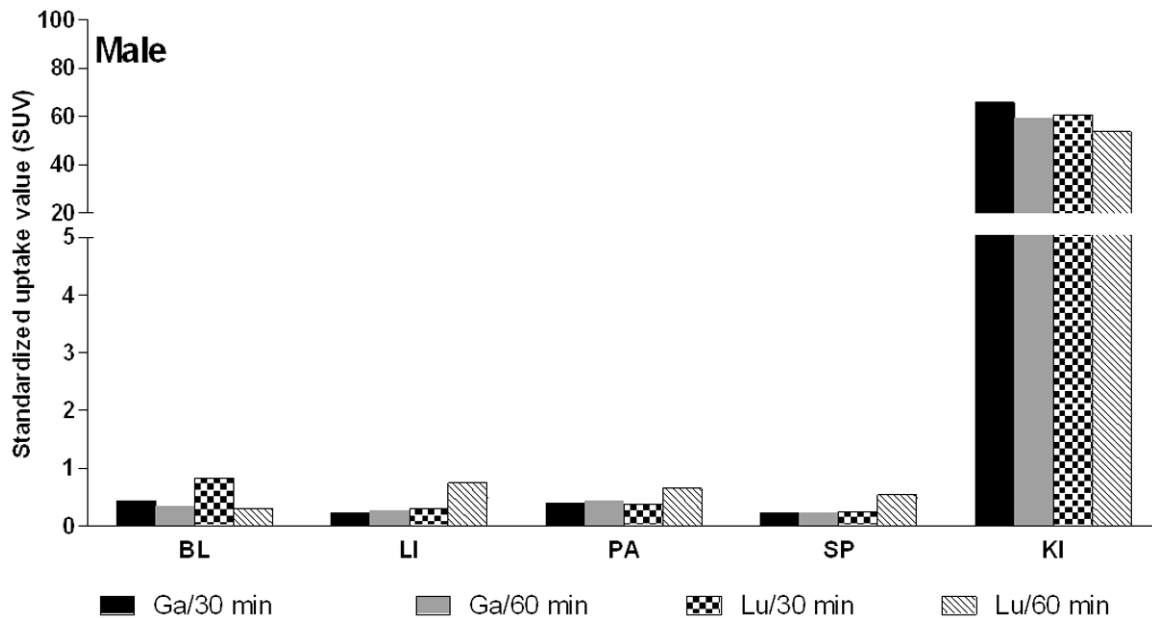
Figure 7. Organ distribution of [^{68}Ga]-DO3A-VS-Cys^{40}-Exendin-4 and [^{177}Lu]-DO3A-VS-Cys^{40}-Exendin-4 in male rats at 0.5 and 1 h p.i. BL: blood; LI: liver; PA: pancreas; SP: spleen; KI: kidneys.

gammas (0.208 MeV (11%) and 0.113 MeV (6.4%)) that can be used for the simultaneous imaging and dosimetry. However the accurate measurement of radioactivity concentrations with SPECT is challenging. The underestimation of absorbed doses in smaller lesions (< 4-5 cm) may occur due to the limited spatial resolution of ^{177}Lu/SPECT images (2 cm). The limited scan number and thus limited data sampling causes inaccuracies due to oversimplification of the underlying kinetics. Moreover, the poor temporal resolution of SPECT precludes the measurement at early time points where the kinetic changes are more pronounced. The quantification accuracy, higher spatial resolution, and dynamic scanning using ^{68}Ga/PET would overcome these disadvantages however the major problem is the mismatch of half-lives of ^{68}Ga and ^{177}Lu that results in different time windows. The possible solution providing highly improved internal dosimetry could be the combined use of both analogues [43]. This approach would also enable evaluation and determination of the feasibility of sole usage of ^{68}Ga-labelled analogue for pre-therapeutic dosimetry and administered radioactivity dose planning. This can be accomplished if the analogues demonstrate similar chemical, physico-chemical and biological properties [2]. Given the vast experience with SST analogues that demonstrated

variability of the biodistribution pattern dependent on the radiometal cation type and other chemical modifications [44], we preliminary compared the biodistribution of [^{68}Ga]-DO3A-VS-Cys^{40}-Exendin-4 and [^{177}Lu]-DO3A-VS-Cys^{40}-Exendin-4.

The comparison of the radioactivity accumulation in the organs of interest investigated at 0.5 and 1 h time points demonstrated similar pattern for [^{68}Ga]-DO3A-VS-Cys^{40}-Exendin-4 and [^{177}Lu]-DO3A-VS-Cys^{40}-Exendin-4 with SUV < 1 for blood, liver, spleen and pancreas (**Figure 7**). Accumulation was not detected in the red bone marrow for either agent. These results indicate that the biodistribution data obtained with [^{68}Ga]-DO3A-VS-Cys^{40}-Exendin-4 might be extrapolated for the dosimetric calculations of [^{177}Lu]-DO3A-VS-Cys^{40}-Exendin-4. However, more thorough investigations are required in order to prove this concept. In addition, the dosimetric calculations in this study were conducted by extrapolation of [^{177}Lu]-DO3A-VS-Cys^{40}-Exendin-4 organ distribution performed in rats, however the absorbed doses of [^{68}Ga]-DO3A-VS-Cys^{40}-Exendin-4 were lower in pig, non-human primate and human as compared to rat [11, 30, 45, 46], and since [^{177}Lu]-DO3A-VS-Cys^{40}-Exendin-4 follows the same biodistribution pattern, the rat data may underestimate the radioactivity dose that can safely be administered.

Conclusions

The biodistribution of [^{177}Lu]-DO3A-VS-Cys^{40}-Exendin-4 in rat was studied as a function of time and the data was used for the calculation of radiation dosimetry in humans. The blood clearance and elimination were fast without accumulation in organs including bone marrow. The dose-limiting organ was kidney with 3.8 GBq of [^{177}Lu]-DO3A-VS-Cys^{40}-Exendin-4 that could be injected before reaching the limit of 23 Gy. However, the preliminary estimation of the respective tumour absorbed dose indicated insufficient values that may render treatment futile. Hypothetically, the kidney protection and peptidase inhibition may allow reduction of kidney absorbed dose and amplification of the tumour absorbed doses. These means are required for possible use of [^{177}Lu]-DO3A-VS-Cys^{40}-Exendin-4 for the dosimetry guided fractionated radiotherapy of insulinomas.

Acknowledgements

Address correspondence to: Dr. Irina Velikyan, PET-Center, Center for Medical Imaging, Uppsala University Hospital, SE-751 85 Uppsala, Sweden. Tel: +46 (0) 70 4834137; Fax: +46 (0) 18 6110619; E-mail: irina.velikyan@bms.uu.se

References

[1]	Fass L. Imaging and cancer: a review. Mol Oncol 2008; 2: 115-152.

[2]	Velikyan I. Radionuclides for Imaging and Therapy in Oncology. In: Chen X, Wong S, editors. Cancer Theranostics. Elsevier; 2014. pp. 285-325.

[3]	Bouchelouche K and Capala J. 'Image and treat': an individualized approach to urological tumors. Curr Opin Oncol 2010; 22: 274-280.

[4]	Bodei L, Cremonesi M, Grana CM, Fazio N, Iodice S, Baio SM, Bartolomei M, Lombardo D, Ferrari ME, Sansovini M, Chinol M and Paganelli G. Peptide receptor radionuclide therapy with 177Lu-DOTATATE: The IEO phase I-II study. Eur J Nucl Med Mol Imaging 2011; 38: 2125-2135.

[5]	Kam BLR, Teunissen JJM, Krenning EP, De Herder WW, Khan S, Van Vliet EI and Kwekkeboom DJ. Lutetium-labelled peptides for therapy of neuroendocrine tumours. Eur J Nucl Med Mol Imaging 2012; 39: S103-S112.

[6]	Garske U, Sandstrom M, Johansson S, Granberg D, Lundqvist H, Lubberink M, Sundin A and Eriksson B. Lessons on Tumour Response: Imaging during Therapy with (177)Lu-DOTA-octreotate. A Case Report on a Patient with a Large Volume of Poorly Differentiated Neuroendocrine Carcinoma. Theranostics 2012; 2: 459-471.

[7]	Kwekkeboom DJ, de Herder WW, Kam BL, van Eijck CH, van Essen M, Kooij PP, Feelders RA, van Aken MO and Krenning EP. Treatment with the radiolabeled somatostatin analog [177 Lu-DOTA 0,Tyr3]octreotate: toxicity, efficacy, and survival. J Clin Oncol 2008; 26: 2124-2130.

[8]	Imhof A, Brunner P, Marincek N, Briel M, Schindler C, Rasch H, Macke HR, Rochlitz C, Muller-Brand J and Walter MA. Response, survival, and long-term toxicity after therapy with the radiolabeled somatostatin analogue [90Y-DOTA]-TOC in metastasized neuroendocrine cancers. J Clin Oncol 2011; 29: 2416-2423.

[9]	De Herder WW, Niederle B, Scoazec JY, Pauwels S, Klöppel G, Falconi M, Kwekkeboom DJ, Öberg K, Eriksson B, Wiedenmann B, Rindi G, O'Toole D, Ferone D, Ahlman H, Arnold R, Bechstein WO, Cadiot G, Caplin M, Christ E, Chung D, Couvelard A, Delle Fave G, Falchetti A, Goretzki P, Gross D, Hochhauser D, Hyrdel R, Jensen R, Kaltsas G, Keleştimur F, Kianmanesh R, Knapp W, Knigge UP, Komminoth P, Körner M, Kos-Kudła B, Kvols L, Lewington V, Lopes JM, Manfredi R, McNicol AM, Mitry E, Nikou G, Nilsson O, O'Connor J, Pape UF, Pavel M, Perren A, Plöckinger U, Ramage J, Ricke J, Ruszniewski P, Salazar R, Sauvanet A, Scarpa A, Sevilla Garcia MI, Steinmüller T, Sundin A, Taal B, Van Cutsem E, Vullierme MP, Wildi S, Yao JC and Zgliczyñski S. Well-differentiated pancreatic tumor/carcinoma: Insulinoma. Neuroendocrinology 2006; 84: 183-188.

[10]	Okabayashi T, Shima Y, Sumiyoshi T, Kozuki A, Ito S, Ogawa Y, Kobayashi M and Hanazaki K. Diagnosis and management of insulinoma. World J Gastroenterol 2013; 19: 829-837.

[11]	Eriksson O, Velikyan I, Selvaraju RK, Kandeel F, Johansson L, Antoni G, Eriksson B, Sörensen J and Korsgren O. Detection of metastatic insulinoma by positron emission tomography with [68Ga]exendin-4-A case report. J Clin Endocrinol Metab 2014; 99: 1519-1524.

[12]	Selvaraju RK, Velikyan I, Asplund V, Johansson L, Wu Z, Todorov I, Shively J, Kandeel F, Eriksson B, Korsgren O and Eriksson O. Pre-clinical evaluation of [68Ga]Ga-DO3A-VS-Cys40-Exen-

din-4 for imaging of insulinoma. Nucl Med Biol 2014; 41: 471-476.

[13] Wicki A, Wild D, Storch D, Seemayer C, Gotthardt M, Behe M, Kneifel S, Mihatsch MJ, Reubi JC, Macke HR and Christofori G. [Lys40(Ahx-DTPA-111In)NH2]-Exendin-4 is a highly efficient radiotherapeutic for glucagon-like peptide-1 receptor-targeted therapy for insulinoma. Clin Cancer Res 2007; 13: 3696-3705.

[14] Li L, Olafsen T, Anderson A-L, Wu A, Raubitschek AA and Shively JE. Reduction of Kidney Uptake in Radiometal Labeled Peptide Linkers Conjugated to Recombinant Antibody Fragments. Site-Specific Conjugation of DOTA-Peptides to a Cys-Diabody. Bioconjugate Chem 2002; 13: 985-995.

[15] Wu Z, Todorov I, Li L, Bading JR, Li Z, Nair I, Ishiyama K, Colcher D, Conti PE, Fraser SE, Shively JE and Kandeel F. In vivo imaging of transplanted islets with 64Cu-DO3A-VS-Cys40-Exendin-4 by targeting GLP-1 receptor. Bioconjug Chem 2011; 22: 1587-1594.

[16] Bolch WE, Eckerman KF, Sgouros G, Thomas SR, Brill AB, Fisher DR, Howell RW, Meredith R and Wessels BW. MIRD pamphlet No. 21: A generalized schema for radiopharmaceutical dosimetry-standardization of nomenclature. J Nucl Med 2009; 50: 477-484.

[17] Loevinger R, Budinger T and Watson E. MIRD Primer for Absorbed Dose Calculations. New York: Society of Nuclear Medicine 1988.

[18] Stabin MG, Sparks RB and Crowe E. OLINDA/EXM: the second-generation personal computer software for internal dose assessment in nuclear medicine. J Nucl Med 2005; 46: 1023-1027.

[19] Sgouros G. Bone marrow dosimetry for radioimmunotherapy: Theoretical considerations. J Nucl Med 1993; 34: 689-694.

[20] Bouchet LG, Bolch WE, Blanco HP, Wessels BW, Siegel JA, Rajon DA, Clairand I and Sgouros G. MIRD Pamphlet No. 19: Absorbed fractions and radionuclide S values for six age-dependent multiregion models of the kidney. J Nucl Med 2003; 44: 1113-1147.

[21] Lewis JS, Wang M, Laforest R, Wang F, Erion JL, Bugaj JE, Srinivasan A and Anderson CJ. Toxicity and dosimetry of 177Lu-DOTA-Y3-octreotate in a rat model. Int J Cancer 2001; 94: 873-877.

[22] Schmitt A, Bernhardt P, Nilsson O, Ahlman H, Kolby L, Schmitt J and Forssel-Aronsson E. Biodistribution and dosimetry of 177Lu-labeled [DOTA0,Tyr3]octreotate in male nude mice with human small cell lung cancer. Cancer Biother Radiopharm 2003; 18: 593-599.

[23] Lewis JS, Laforest R, Lewis MR and Anderson CJ. Comparative dosimetry of copper-64 and yttrium-90-labeled somatostatin analogs in a tumor-bearing rat model. Cancer Biother Radiopharm 2000; 15: 593-604.

[24] De Jong M, Breeman WAP, Bernard BF, Bakker WH, Schaar M, Van Gameren A, Bugaj JE, Erion J, Schmidt M, Srinivasan A and Krenning EP. [177Lu-DOTA0,Tyr3]octreotate for somatostatin receptor-targeted radionuclide therapy. Int J Cancer 2001; 92: 628-633.

[25] Sandstrom M, Garske-Roman U, Granberg D, Johansson S, Widstrom C, Eriksson B, Sundin A, Lundqvist H and Lubberink M. Individualized dosimetry of kidney and bone marrow in patients undergoing 177Lu-DOTA-octreotate treatment. J Nucl Med 2013; 54: 33-41.

[26] Wehrmann C, Senftleben S, Zachert C, Muller D and Baum RP. Results of Individual Patient Dosimetry in Peptide Receptor Radionuclide Therapy with 177Lu DOTA-TATE and 177Lu DOTA-NOC. Cancer Biother Radiopharm 2007; 22: 406-416.

[27] Kwekkeboom DJ, Bakker WH, Kooij PP, Konijnenberg MW, Srinivasan A, Erion JL, Schmidt MA, Bugaj JL, de Jong M and Krenning EP. [177Lu-DOTAOTyr3]octreotate: comparison with [111In-DTPAo]octreotide in patients. Eur J Nucl Med 2001; 28: 1319-1325.

[28] Ban K, Noyan-Ashraf MH, Hoefer J, Bolz SS, Drucker DJ and Husain M. Cardioprotective and vasodilatory actions of glucagon-like peptide 1 receptor are mediated through both glucagon-like peptide 1 receptor-dependent and -independent pathways. Circulation 2008; 117: 2340-2350.

[29] Korner M, Stockli M, Waser B and Reubi JC. GLP-1 receptor expression in human tumors and human normal tissues: potential for in vivo targeting. J Nucl Med 2007; 48: 736-743.

[30] Selvaraju RK, Velikyan I, Johansson L, Wu Z, Todorov I, Shively J, Kandeel F, Korsgren O and Eriksson O. In vivo imaging of the glucagonlike peptide 1 receptor in the pancreas with 68Ga-labeled DO3A-exendin-4. J Nucl Med 2013; 54: 1458-1463.

[31] Duncan JR, Stephenson MT, Wu HP and Anderson CJ. Indium-111-diethylenetriaminepentaacetic acid-octreotide is delivered in vivo to pancreatic, tumor cell, renal, and hepatocyte lysosomes. Cancer Res 1997; 57: 659-671.

[32] Rolleman EJ, Melis M, Valkema R, Boerman OC, Krenning EP and De Jong M. Kidney protection during peptide receptor radionuclide therapy with somatostatin analogues. Eur J Nucl Med Mol Imaging 2010; 37: 1018-1031.

[33] Melis M, Bijster M, De Visser M, Konijnenberg MW, De Swart J, Rolleman EJ, Boerman OC, Krenning EP and De Jong M. Dose-response effect of Gelofusine on renal uptake and retention of radiolabelled octreotate in rats with CA20948 tumours. Eur J Nucl Med Mol Imaging 2009; 36: 1968-1976.

[34] Valkema R, Pauwels SA, Kvols LK, Kwekke-boom DJ, Jamar F, De Jong M, Barone R, Wal-rand S, Kooij PPM, Bakker WH, Lasher J and Krenning EP. Long-term follow-up of renal func-tion after peptide receptor radiation therapy with 90Y-DOTA0,Tyr3-octreotide and 177Lu-DOTA0,Tyr3-octreotate. J Nucl Med 2005; 46: 83S-91S.

[35] Barone R, Borson-Chazot F, Valkema R, Wal-rand S, Chauvin F, Gogou L, Kvols LK, Krenning EP, Jamar F and Pauwels S. Patient-specific dosimetry in predicting renal toxicity with (90)Y-DOTATOC: relevance of kidney volume and dose rate in finding a dose-effect relationship. J Nucl Med 2005; 46 Suppl 1: 99S-106S.

[36] Gotthardt M, Van Eerd-Vismale J, Oyen WJG, De Jong M, Zhang H, Rolleman E, Maecke HR, Béhé M and Boerman O. Indication for differ-ent mechanisms of kidney uptake of radiola-beled peptides. J Nucl Med 2007; 48: 596-601.

[37] Cremonesi M, Ferrari M, Bodei L, Tosi G and Paganelli G. Dosimetry in peptide radionuclide receptor therapy: A review. J Nucl Med 2006; 47: 1467-1475.

[38] Beauregard JM, Hofman MS, Kong G and Hicks RJ. The tumour sink effect on the biodistribu-tion of 68Ga-DOTA-octreotate: implications for peptide receptor radionuclide therapy. Eur J Nucl Med Mol Imaging 2012; 39: 50-56.

[39] Nock BA, Maina T, Krenning EP and de Jong M. "To serve and protect": enzyme inhibitors as radiopeptide escorts promote tumor targeting. J Nucl Med 2014; 55: 121-127.

[40] Hupe-Sodmann K, McGregor GP, Bridenbaugh R, Goke R, Goke B, Thole H, Zimmermann B and Voigt K. Characterisation of the processing by human neutral endopeptidase 24.11 of GLP-1(7-36) amide and comparison of sub-strate specificity of the enzyme for other gluca-gon-like peptides. Regul Pept 1995; 58: 149-156.

[41] Simonsen L, Holst JJ and Deacon CF. Exen-din-4, but not glucagon-like peptide-1, is cleared exclusively by glomerular filtration in anaesthetised pigs. Diabetologia 2006; 49: 706-712.

[42] Plamboeck A, Holst JJ, Carr RD and Deacon CF. Neutral endopeptidase 24.11 and dipeptidyl peptidase IV are both mediators of the degra-dation of glucagon-like peptide 1 in the anaes-thetised pig. Diabetologia 2005; 48: 1882-1890.

[43] Velikyan I. Prospective of 68Ga-Radiopharma-ceutical development. Theranostics 2014; 4: 47-80.

[44] Velikyan I. Positron emitting [^{68}Ga]Ga-based imaging agents: chemistry and diversity. Med Chem 2011; 7: 338-372.

[45] Nalin L, Selvaraju RK, Velikyan I, Berglund M, Andreasson S, Wikstrand A, Ryden A, Lubber-ink M, Kandeel F, Nyman G, Korsgren O, Eriks-son O and Jensen-Waern M. Positron emission tomography imaging of the glucagon-like pep-tide-1 receptor in healthy and streptozotocin-induced diabetic pigs. Eur J Nucl Med Mol Im-aging 2014; 41: 1800-10.

[46] Bulenga TN, Selvaraju R, Estrada S, Asplund V, Lubberink M, Velikyan I and Eriksson O. Dosim-etry of 68Ga and 177Lu labeled Exendin4 - im-pact on feasibility of repeated PET imaging and radiotherapy. Paper presented at: EANM, 2014.